Indentation deformation and cracking behavior of hydrated aluminoborate glasses

Liu, Pengfei; Jensen, Lars R.; Gao, Chengwei; Smedskjaer, Morten M.

Published in:
Journal of the American Ceramic Society

DOI (link to publication from Publisher):
10.1111/jace.18175

Publication date:
2022

Document Version
Accepted author manuscript, peer reviewed version

Indentation deformation and cracking behavior of hydrated aluminoborate glasses

Pengfei Liu[1], Lars R. Jensen[2], Chengwei Gao[1], Morten M. Smedskjaer[1,*]

[1]*Department of Chemistry and Bioscience, Aalborg University, Aalborg, Denmark*

[2]*Department of Materials and Production, Aalborg University, Aalborg, Denmark*

[*] Corresponding author. e-mail: mos@bio.aau.dk

Abstract

Aluminoborate glasses have recently been found to feature high resistance to crack initiation during indentation due to a highly flexible network structure. In cesium aluminoborate glasses, it has been found that the use of a simple post-treatment, namely aging in a humid atmosphere, can further improve this resistance. To better understand the mechanical properties of this glass family upon humid aging, we here study the effect of aging conditions on the structure and mechanical properties of Li,K,Cs-aluminoborate glasses. As expected, we find that higher humidity and longer aging time cause more pronounced permeation of atmospheric water into the glasses. Due to their denser structure and stronger modifier-oxygen bonds, the humid aging has a relatively smaller effect on the mechanical properties of Li- and K-containing glasses relative to Cs-containing glasses, with the latter achieving an ultrahigh crack resistance. We find that the humid aging leads to the formation of a hydration layer in the Cs-aluminoborate glass surface, with a thickness of around 26 µm upon aging at 23 ℃ with 40% relative humidity for 7 days. Moreover, we report a remarkable indentation behavior, i.e., observation of µm-sized shear bands inside the imprint of the Cs-glass upon aging at 60% relative humidity. Taken as a whole, our work provides guidelines for how to control the humid aging rate as a function of relative humidity and temperature to form a hydration layer and thus achieve ultrahigh crack resistance in such glasses.

1. Introduction

Borate-based glasses are important engineering and functional materials due to their excellent properties,[1,2] such as good bioactivity, high transparency, and low melting temperature. However, the

This article has been accepted for publication and undergone full peer review but has not been through the copyediting, typesetting, pagination and proofreading process, which may lead to differences between this version and the Version of Record. Please cite this article as doi: 10.1111/18175.

obvious drawback of these glasses is their relatively low chemical durability[2,3,4] due to the high surface reactivity in atmospheric humidity environments. This high surface reactivity can lead to the surface corrosion and hydration, which significantly influence various important glass properties, from mechanics[5-9] (strength and cracking behavior) to optics (transparency)[10] and thermal behavior (glass transition temperature).[11,12] Particularly the mechanical properties are crucial for many oxide glass applications. Understanding the details of glass-water interactions is thus crucial for tailoring the mechanical performance of borate glasses.

Glasses typically fail due to the presence of surface cracks and defects, which in turn arise from corrosion, impacts and scratch events during production and daily use. These defects amplify the local tensile stress, which can result in decreasing the practical strength and lead to catastrophic failure. From Griffith-Irwin's fracture criterion,[13] we know that flaws with a critical size can only grow under loads that exceed the static fatigue limit.[14] Some works[14,15] have found that a lower applied loading rate will result in a larger contribution of sub-critical crack growth to the fracture process. That is because lower loading rate allows more time for the stress corrosion from water, thus leading to the lower practical strength. Since the main factor affecting stress corrosion from water is the diffusion of water to the crack tip, the diffusion rate of water in glasses is also considered to be one of the important factors affecting its structure and mechanics.[16,17,18,19] Recent work have shown that the diffusion rate of water in the glass will change with the applied load.[20,21] An applied compressive stress will enhance the rate of water penetration into the glass.[20,21] Therefore, it is of great significance to study the influence of water penetration in glasses on the mechanical properties under different hydration conditions.

In general, water penetration can decrease the practical strength of glasses, but the hydration surface treatment can in some cases enhance the crack initiation and crack growth resistance in glasses.[20-24] For example, it has been shown that water penetration into the glass surface can cause expansion below the surface, and thus create a layer of compressive stress.[23] This compressive stress layer has the effect that any applied tension needs to overcome the existing surface compression, thereby improving the surface damage resistance. Some works have found that water penetration in

glass can resist crack growth by shielding the crack tip due to network swelling.[7] Moreover, pre-hydration of the glass surface can increase their crack initiation resistance (*CR*) under sharp contact loading. The study of Gross *et al.*[24] showed an increase in *CR* from 50 to 100 N of some phosphoaluminosilicate glasses upon aging at 22 °C at 85% relative humidity (RH) for 30 days.

As such, it is well known that many environmental factors (such as pressure, temperature, and RH) affect the rate of water penetration. To clarify the relation between the extent of water penetration (as tuned by the glass composition) and *CR*, we here study the indentation cracking behavior of different alkali aluminoborate glasses subjected to varying hydration conditions. We focus on aluminoborate glasses[20,21,25] as they are well known for their the soft and highly adaptable network structure and relatively low chemical durability compared to silicate glasses. These characteristics allow easier water penetration in aluminoborate glasses that will have a significant impact on their mechanical properties. Specifically, we study the chemical durability and aging-induced water content in three different aluminoborate glasses ($25M_2O$-$25Al_2O_3$-$50B_2O_3$ with M = Li, K, Cs), which have different chemical durability (Li-glass most durable, Cs-glass least durable) due to the difference in modifier field strength. Micro-indentation is performed on all hydrated surfaces to study the role of hydration on deformation phenomena, including elastic recovery, indent size length recovery, indentation-induced shear bands, and crack initiation. Finally, in the case of the Cs-containing glass, we measure the depth of the hydration layer based on micro-Raman spectroscopy analysis.

2. Experimental

2.1 Glass preparation

We used the traditional melt-quenching technique to prepare the three different aluminoborate glasses with the composition $25M_2O$-$25Al_2O_3$-$50B_2O_3$ (in mol%) for M = {Li, K, Cs}. These glasses are named LiAlB, KAlB, and CsAlB, respectively. The utilized raw materials were Li_2CO_3 (≥98.5%, Merck KGaA), K_2CO_3 (≥99.5%, Merck KGaA), Cs_2CO_3 (99.5%, Sigma-Aldrich), Al_2O_3 (99.5%, Sigma-Aldrich), and H_3BO_3 (≥99.5%, Honeywell International). All raw materials were weighed and thoroughly mixed in a glass bottle. To remove the excess H_2O and CO_2, the mixed batch were

stepwise added into a Pt-Rh crucible and heated at 500 °C in an electric furnace (Entech). Then, the mixed powders were melted for 2 hours in air at 1070 ℃ for CsAlB, 1300 ℃ for KAlB, and 1400 ℃ for LiAlB, and the melted batch was poured onto a steel plate for quenching.

We moved the obtained glasses into a preheated annealing furnace at an estimated glass transition temperature (T_g) based on the previous studies[21,25,26]. Subsequently, the T_g of the glasses was determined from diff erential scanning calorimetry measurements (STA 449 F3 Jupiter, Netzsch) at 10 K/min on specimens with a preceding cooling rate of 10 K/min. These glasses were analyzed using Pt crucible in argon (gas flow 60 mL/min). T_g and other property data of studied glasses are summarized in Table S1 in the Supporting Information. Subsequently, all obtained glasses were re-annealed for 30 min at their measured-T_g and cooled down to room temperature at a cooling rate of around 3 K/min. After the re-annealing process, all glasses were cut for the subsequent characterization experiments (see below) and then optically polished in ethanol by using abrasive SiC disks (up to grit 4000). All samples were then kept in a desiccator to avoid surface hydration.

X-ray diffraction (XRD) patterns of the specimens were acquired (Empyrean XRD, PANalytical) from 5° to 80° at 40 kV with a scanning speed of 8 °/min. From Figure S1 in the Supporting Information, we do not observe any signs of crystallization or phase separation in all glasses.

2.2 Humid aging post-treatment

All studied glasses were subjected to surface hydration through controlled humid aging experiments in a climate chamber (WKL 100/40, Weiss). All samples were optically double-side polished in ethanol, and then were immediately put into the climate chamber. The aging experiment was performed at different temperatures and RHs for up to 7 days (see detailed treatment conditions in Table S2 in the Supporting Information). For the CsAlB glass, it was found that the glass surface was cracked after 6 hours of aging at 23 ℃ and 60% RH. Therefore, the aging experiment for the CsAlB glasses was only done at 23 ℃ with 40% RH and 50% RH, respectively, for varying duration up to 7 days. Furthermore, to investigate the hydration in a high-humidity environment, experiments were

also performed at 120 ℃ with 100% RH for 30 min in an autoclave. For the CsAlB glasses, the aging experiment was also performed in 99.9% ethanol for up to 14 days.

2.3 Infrared spectroscopy

To study the content and form of water in the as-prepared glasses before/after humid aging, we performed attenuated total reflection infrared (ATR-IR) spectroscopy measurements on the double-side polished bulk samples with the same size (10×10×5 mm). The ATR-IR spectra were acquired using a Spectrum One spectrometer (PerkinElmer STA 6000) on a Ge ATR crystal under ambient conditions with subsequent background subtraction. We measured at least five different positions of each sample to reduce the error. Furthermore, to achieve more detailed information on the water content of the studied glasses after humid aging, we performed thermogravimetric analysis (TGA) measurements (STA 449 F3 Jupiter, Netzsch) at a heating/cooling rate of 10 K/min on powder glass samples with the same mass (2 g) and similar particle size (≤ 45 μm). These samples were analyzed using Pt crucible in argon (gas flow 60 mL/min).

2.4 Density

We determined the density (ρ) of all studied glasses by using Archimedes' principle of buoyancy. The weight of each specimen (at least 2.5 g) was measured in air and 99.9% ethanol at least ten times. Based on the ratio between molar mass and density, we also calculated the molar volume (V_m) and the atomic packing density (C_g) to quantify differences in free volume among the studied glasses. This was done by assuming 6-fold coordination for modifier atoms (Li, K and Cs), 2-fold coordination for O, 3-fold and 4-fold coordination for B, and 4-fold, 5-fold and 6-fold coordination for Al (based on information from previous NMR analyses[21,26]).

2.5 UV-VIS spectroscopy

To quantify whether the humid aging treatment affects the visual appearance of the glasses, we determined the optical transparency of 2.0 mm thick glass samples. The analysis was done using an

ultraviolet-visible (UV-VIS) spectrometer (Cary 50 Bio, Varian), with transmission spectra collected every day in the wavelength range between 255 and 800 nm. We measured at least five different positions of each sample to ensure homogeneity. The distance between each position was at least 2 mm. All the UV-VIS transmittance spectra were normalized to 1 mm thickness.

2.6 Chemical durability

To compare the chemical durability of the three annealed glasses in water, we cut three rectangular specimens with dimensions of 10×10×5 mm^3 from each bulk glass. The all-side polished specimens were then ultrasonicated in distilled water for 5 min, and then in acetone for 5 min, followed by drying at 105 °C. The mass and surface area of each specimen was recorded and the specimens were then immersed in aqueous solutions at pH = 7 (pH adjusted by HCl and NaOH) at room temperature. The specimens were systematically withdrawn from the aqueous solutions as a function of time and then dried at 105 °C, weighed, and re-immersed in the solutions. We measured the mass loss of Li, K-aluminoborate glasses 7 times within 168 hours due to the high chemical durability, while we measured the mass loss of Cs-aluminoborate glasses 5 times within 8 hours due to the low chemical durability. The dissolution rate was determined from the correlation between mass loss (normalized to the initial surface area) and time. The glass-to-liquid ratio was selected to be low enough to avoid any saturation effects, i.e., the weight loss is linear with time.

2.7 Raman spectroscopy

To quantify the depth of water penetration into the as-prepared CsAlB glass upon humid aging, we performed micro-Raman spectroscopy measurements on the double-side polished bulk samples with the same size (10×10×5 mm^3). To avoid further hydration after the pre-determined aging treatment, we chose this method, since the measurement is fast and could be performed immediately after the treatment. Raman spectra were collected on an inVia micro-Raman spectrometer (Renishaw) with an objective with a numerical aperture of 0.75, a 532 nm laser, an acquisition time of 10 s and in a high confocality mode ensuring increased lateral spatial resolution. The range of all spectra was from 220

to 4000 cm^{-1}, with a resolution better than 2 cm^{-1}. The Raman spectra were collected on the surface and at increasing depths from the top surface of the hydrated CsAlB glasses by moving the digital controlled microscope table upwards. In this study, the optical resolution of micro-Raman was estimated to be around 0.8 μm in X,Y-stage and 1.9 μm in Z-stage. Each step distance of Z-stage was at least 2 μm in the measurements and we measured the hydration layer depth at five different positions of each sample for the error analysis. All spectra were uniformly treated for background correction and area normalization.

2.8 Micro-indentation experiments

The Vickers hardness (H_V) and crack initiation resistance (*CR*) of all studied glasses were determined by using a Nanovea CB500 microindenter (Irvine, California). For each sample, at least 15 Vickers indents with a load of 9.8 N (1 kgf) were generated to determine H_V as described elsewhere[21]. The loading duration and dwell time were set to 6 s and 10 s, respectively. To evaluate *CR*, all samples were indented at different loads (at least five) using Vickers diamond tip geometries. According to the method of Wada *et al.*[27], the probability of crack initiation (PCI) at each load was derived as the ratio between the number of corners with a corner crack and the total number of corners. The crack resistance is defined as the load at which an average of 2 cracks per indent (PCI =50%) occurred. For each load, at least 15 indents were made by using the Vickers indenter tip. The loading duration of 6 s was used for loads below 45 N, but for the higher loads, the loading rate becomes too fast for this and was instead fixed at 7.5 N/s, with the same dwell time of 5 s. The measurements were conducted under laboratory conditions (room temperature and RH of 40-45%).

We also evaluated the change in the indents size as a function of time by determining the bow-in parameter (L_D/L_S ratio, where L_D is indent diagonal length and L_S is opposite side length), and the recovery of the indent side length. To do so, all samples were first indented 15 times by a Vickers tip at a load of 9.8 N with a loading duration of 6 s and dwell time of 10 s. Then images of the indents were recorded using the built-in microscope. After indentation and imaging, these samples were transferred to the climate chamber for aging at 23 °C with 40%, 50%, 60%, or 80% RH, and then the

existing indents were imaged once every day. The initial (20-30 s after unloading) indentation side length, $L_{s,i}$, was determined and then determined again after aging, $L_{s,a}$. We then employ an approach that is similar to the method for recovery of indentation volume to estimate densification contribution to overall indentation deformation.[28,29] That is, we calculate the aging-induced side length recovery (L_{AR}) as,

$$L_{AR} = \frac{L_{s,i} - L_{s,a}}{L_{s,i}}. \quad (1)$$

3. Results

3.1 Chemical durability

To better understand the differences in humid aging behavior of the three alkali aluminoborate glasses, we have measured the chemical durability of the bulk glasses in neutral (pH = 7) solutions. Figure S2 in the Supporting Information shows the weight loss normalized by the initial surface area of all studied glasses as a function of immersion time. As there is no saturation in the solutions, the weight loss curves exhibit a linear time dependence, with no plateau in the weight loss. From the slope of each curve, we then derive the dissolution rate (D_r, in mg dm^{-2} h^{-1}). The dissolution behavior depends on various factors such as atomic packing density, the rigidity of the network, modifier field strength, content of network formers, and the network former speciation. Furthermore, we find from our previous work[26,30] that the rigidity of the network is strongly related to the modifier field strength in borate and aluminoborate glasses. In this study, the aluminium-to-boron ratio is kept constant and we thus investigate the alkali field strength and atomic packing density dependence of dissolution rate. The modifier field strength (*FS*) can be quantitatively determined as defined by Dietzel[31]:

$$FS = \frac{z_{alkali}}{(r_{alkali} + r_{oxygen})} \quad (2)$$

where *z* and *r* are the charge and the ionic radius, respectively.

Figure 1 shows the *FS* and C_g dependence on the logarithmic dissolution rate for all studied glasses in the neutral (pH = 7) solutions. From Figure 1a, we can find that the dissolution rate decreases with the increase in alkali field strength. This is because modifier cations with high-field strength form stronger bonds with oxygen with higher dissociation energy[32,33] (under the same aluminium-to-boron ratio condition). This result is well in agreement with the expected relation between field strength and dissolution kinetics, where the degree of leaching of alkali modifier ions increases with decreasing *FS* in aluminoborate glasses[34]. This result shows that the Cs-O bonds may be more susceptible to the nucleophilic attack of the H_2O molecule (hydrolysis)[21] than the other two glasses during the hydration process. Figure 1b also shows that the aluminoborate glass with the lower-*FS* Cs_2O modifier has a lower atomic packing density. This is because: (1) smaller modifiers can more efficiently fill the voids left between O atoms, thereby reducing the amount of internal free volume, and (2) modifiers exhibiting large *FS* tend to attract the surrounding O atoms more, thereby forcing them to partially overlap with each other[26,35]. Thus, D_r decreases with increasing C_g. These loose network structures are conducive to the entry of water molecules into the glass, resulting in the nucleophilic attack of H_2O molecule (hydrolysis). Overall, the results in Figure 1 indicate that the hydration behavior should be affected by the network free volume and the modifier bond strength.

3.2 Water content

In general, there are three main mechanisms for water entry into glasses: (1) hydration (molecular water penetration into the glass network), (2) hydrolysis (reaction with the glass network), and (3) leaching (ion-exchange reaction with modifier cations). Water typically exists in glasses in the form of either molecules or hydroxyl groups.[36,37,38] To determine the content and form of water in studied glasses, we use ATR-IR spectroscopy on the glass samples upon the humid aging treatments. Figures 2a-c show the ATR-IR spectra of LiAlB, KAlB, CsAlB glasses with different aging time at different RHs. For the KAlB and CsAlB glasses, the water is mainly present in the form of the OH stretching band (ν_{OH}, ~3400 cm^{-1}), with a small amount of molecular H_2O bending band (δ_{H2O}, ~1620 cm^{-1}) in these glasses. Due to the higher chemical durability, we can only find the water in the form of the OH

stretching band in the LiAlB glass. To quantify the changes in the hydroxyl groups with the aging time in the three glasses, we consider the relation between the relative intensity of OH stretching band (ν_{OH}) and humid aging time (Figure 2d). This intensity of for the LiAlB and KAlB glasses increases after humid aging under high RHs. On the other hand, the humid aging process only has a minor effect on the water content in the LiAlB and KAlB glasses under low RHs (40% and 60% RH) as shown in Figure S3. For the CsAlB glass, the relative intensity of OH stretching band increases significantly after humid aging even under low RHs (40% and 50% RH), indicating that the humid aging process has a significant influence on the surface of CsAlB glass.

The TGA analysis supports these conclusions (see Figure S4 in the Supporting Information). That is, the water contents of the lithium and potassium aluminoborate glasses are below 1 wt% under different conditions. The powdered glasses have a large propensity for water uptake due to the larger surface-to-volume ratio and, as such, these results imply that the surfaces of bulk LiAlB and KAlB glasses only undergo limited surface hydration. On the contrary, the humid aging process has a significant influence on the surface of CsAlB glass, i.e., the water content of the cesium aluminoborate glass increases with increasing humidity. The water content is around 12 wt% after 7-days aging when the relative humidity is 60%. In general, the trend in water uptake follows the trend in chemical durability (Fig. 1) among the three glasses.

3.3 Hydration layer depth

From the water content analysis above, we found that most water penetrates into the CsAlB glasses upon humid aging. We therefore focus on this glass composition when investigating the time dependence of the depth of the hydration layer by using micro-Raman spectroscopy. The lowest frequency band region Ⅰ, ranging from ~280 to 625 cm^{-1}, is related to the contributions from B-O-B, Al-O-Al, and B-O-Al stretching vibrations, as well as the vibrations due to superstructural units such as pentaborates. Furthermore, the band region Ⅱ, ranging from ~2850 to 3800 cm^{-1}, is associated with hydroxyl groups attached to the glass network due to hydration[26,27]. As observed in Figure 3a, the band region Ⅰ hardly changes upon aging. Therefore, we choose to calculate the area ratio of band

regions Ⅰ and Ⅱ to capture the change in water content of CsAlB glass with increasing depth (Figure 3b). To estimate the boundary between the hydration layer and the original glass, we fit the experimental data to an exponential function (solid line) and the hydration layer is defined as the depth for which the slope of the curve is less than -0.01 μm^{-1}. Since the initial bulk glass inevitably contains some water, we have not used a value 0 μm^{-1}, but chosen -0.01 μm^{-1}. We have tried using different threshold values, but it only slightly changes the depth values and does not influence the conclusions from the analysis. Based on this calculation methodology, we have calculated the hydration layer depth in the CsAlB glasses as a function of humid aging time under different RHs (Figure 3c). We observe a positive correlation between hydration layer depth and both the duration of aging as well as RH. This agrees with the variation in total water content for this glass. Especially, we note that a large fraction of the hydration occurs during the very early stages of aging (i.e., 13-14 μm hydration layer after humid aging for 1 day). After 7 days aging at 40% and 50% RH, the main hydration layer depth is 26.4 μm and 29.2 μm, respectively, showing that the high-RH atmosphere increases the hydration rate.

3.4 Elastic recovery during indentation

In our recent work[20,21], we have found that even the indents in the CsAlB glass recorded immediately (20-30 s) after unloading do not show the perfect square shape, indicating obvious recovery already during the unloading process. Furthermore, we know that for the CsAlB glass, a large fraction of the indent size recovery ("self-healing") occurs during the very early stages of the aging (i.e., first data point after unloading). Therefore, it is interesting to study the effect of water penetration degree on the elastic recovery of these glasses.

Both plastic and elastic deformation take place during indentation (see Figure S5), which strongly affects the indentation behavior. Peter showed that the plastic deformation mechanism of oxide glasses in general includes both shear flow and densification[39], with the simple notion that shear flow is the dominant process for compact glasses, whereas densification becomes increasingly important in more open glasses[28,40]. We observed in Figure S5b that the elastic part decreases with

increasing alkali modifier *FS*. The elastic contribution to the total work for the CsAlB glass is about 72%, indicating that elastic deformation has a high contribution to the total deformation during the indentation process compared to most other oxide glasses[41], even relative to metal-organic framework glasses with weak coordination bonding[42]. This observation agree with the finding that amorphous silica with a very open network (i.e., low C_g) displays a relatively pronounced elastic recovery, while densely packed fluoride glasses generally display a low extent of elastic recovery[43]. Based on the optical micrographs analysis of Vickers indents (see Figure S6 in the Supporting Information), we find that there are no pronounced edges of Vickers indents on the surface of the CsAlB glass, implying that sinking-in occurs during loading[44] and high elastic recovery occurs during unloading[43]. This result also supports the above point that elastic deformation has a relatively high contribution to the indentation deformation in the CsAlB glass.

The bow-in parameter (L_D/L_S ratio, where L_D is indent diagonal length and L_S is opposite side length[45]) of Vickers indents can also be used to describe the contribution of elastic deformation to indentation-induced deformation[26]. Figure 4 shows the dependence of L_D/L_S of Vickers indents produced at 9.8 N on the humid aging time for different glasses and different RHs. First, we observe a negative correlation between L_D/L_S ratio and *FS*. That is, the CsAlB glass with the lowest modifier field strength has the highest L_D/L_S ratio and thus undergoes the largest extent of elastic recovery during unloading, which is in agreement with the trend in elastic-induced depth-recovery (Figure S5b). Furthermore, since only relatively few water molecules enter into the glass surfaces of LiAlB and KAlB glasses, there is only a minor change in their L_D/L_S ratio upon humid aging. On the other hand, the bow-in parameter for the CsAlB glass increases with increasing aging time and atmospheric humidity, which is in agreement with the larger extent of water entry in this glass (Figure 2). This indicates that the atmospheric water entry helps to promote the elastic recovery during unloading.

3.5 Indent size length recovery

To evaluate the effect of aging time on the indentation deformation behavior of the three glasses, we have measured the change in the size of the Vickers indent as a function of aging time. Figure S6 in

the Supporting Information shows the optical images of 9.8 N indents on the glass surfaces before and after aging for 7 days at 50 to 80% RH. The indent in CsAlB glasses exhibits significant shrinkage upon 7-days aging (even at relatively low humidity) compared to the LiAlB and KAlB glasses. Furthermore, we note that the edge of this indent appears to have recovered above the original glass surface, in agreement with previous findings for a similar composition[20]. The rate of indentation recovery is then quantified from the aging time dependence of the recovery of the indentation side length (L_{AR}), as shown in Figure 5. We find only limited indent size recovery in the LiAlB glass upon humid aging, in agreement with the results of the bow-in parameter (Figure 4). We ascribe this to the glass' dense and rigid structure, which allows for less water penetration (Figure 2) and thus less indent volume recovery[20]. The KAlB glass exhibits side length recovery above 7% and 15% after 7-days aging at 60% and 80% RH, respectively, while the CsAlB glass exhibits recovery of around 25% and 40% after 7-days aging at 40% and 50% RH, respectively. A large fraction of the recovery for the CsAlB glass occurs during the very early stages of the aging (i.e., first data point after unloading), but the shrinkage gradually continues even after 7 days of aging. This is because the atmospheric water permeates into the glass at a high rate during the very early stages of the aging (Figure 2), which also results in larger indent recovery during unloading (Figure 4).

3.6 Vickers hardness

Figure 6 shows the humid aging time dependence of Vickers hardness. First, H_V of the aluminoborate glasses increases with increasing modifier *FS*, i.e., H_V increases from ~2.5 to ~4.7 GPa when Li_2O is substituted for Cs_2O. Besides the stronger Li-O bonds relative to K-O and Cs-O, H_V also depends on the number of atomic constraints per volume, thus also related to the atomic packing density C_g[46]. This shows that the surface of the CsAlB glass is softer than that of the two other glasses. Hydration under different conditions only has a minor effect on H_V of LiAlB and KAlB glasses, in the agreement with the above results. However, for CsAlB glasses, H_V first increases slightly with the aging time in the early stage of the aging at 50% RH, and subsequently decreases slightly with the aging time. This is likely due to atmospheric water initially permeating into the glass at a high rate, resulting in larger

indent recovery induced by water permeation (not elastic part) during unloading, and thus smaller residual imprint and a higher apparent hardness. The rate of atmospheric water permeation decreases with aging time, resulting in the smaller relative recovery during unloading, and thus lower apparent hardness. According to the chemical durability and water content analysis, we know that the rate of atmospheric water permeation at 50% RH is higher than that at 40% RH. Therefore, the hydration process has a smaller effect on the Vickers hardness of CsAlB glasses for 40% RH. Finally, we note that above results depends on the indentation load, as the use of a smaller indentation load would likely lead to a larger impact of hydration on hardness, since the hydration layer would constitute a larger fraction of the indented region.

3.7 Crack initiation resistance

To understand the cracking behavior of the alkali aluminoborate glasses under sharp contact loading, we here systematically study the effect of surface hydration on the crack initiation behavior of both freshly polished surfaces and those that have undergone humid aging at different conditions for up to 7 days (Figure 7). The humid aging process has only a minor effect on the *CR* of LiAlB and KAlB glasses. This agrees with the relatively small extent of water penetration in these glasses (Figure 2). However, *CR* of the CsAlB glasses increases significantly upon aging at both 40% and 50% RH. We note that the pre-aging *CR* value is lower than that of the previously studied peralkaline caesium aluminoborate glass[21] due to the small difference in the test atmospheric humidity and compositions. During humid aging, the network should expand as the intact dense network is converted to a looser hydrolyzed network, resulting in the increase of *CR*. However, when the aging time reaches 5 days, *CR* of the CsAlB glasses reaches an apparent maximum value for 50% RH. That is probably because that the hydrated surface after long-term aging becomes sufficiently depolymerized to decrease *CR* due to the weaker network bonding and the higher humidity can lead to a higher rate of atmospheric water permeation into the glasses surface. This suggests that the lower rate of atmospheric water permeation is beneficial to achieve hydration layer with an improvement of the crack initiation

resistance of the CsAlB glasses. However, we note that it comes with the sacrifice of lower hardness and lower chemical durability of this glass.

Based on the indent size length recovery analysis, we find a pronounced aging-induced indent recovery in the CsAlB glass within a short time (3 hours) upon aging at 60% RH. As the rate of atmospheric water permeation into the glass surface affects the *CR*, we have also analyzed the indentation behavior of the CsAlB glass upon aging at a higher humidity (60% RH). Figure 8 shows the optical top-view images of Vickers indents produced at different loads on the surface of the CsAlB glass that has been aged at 60% RH for different durations. We observe apparent slip lines inside the indent and pile-up around the indent edges (Figure 8b). Slip lines are typically observed in metallic glasses[47,48] and even some modified oxide glasses[49], indicating the formation of the stepped μm-sized shear bands by the sliding of the stepped structure during indentation. Furthermore, the observation of pile-up around the indent edges can indicate that some isochoric shear flow has been activated during indentation. The formation of a shear band must be caused by a translational motion of structural units[50], which in turn could be due to the formation of the Cs-OH groups and non-ring trigonal boron units[21] with higher degree of freedom and mobility upon humid aging. At a higher indentation load (40 N), we observe apparent pile-up and some edge and radial cracks and dissociation of the hydration layer and glass around the indent (Figure 8d), suggesting that the hydrated CsAlB surface, even after short time of aging, becomes significantly depolymerized due to the weaker network bonding. This result indicates that the high rate of water penetration at 60% RH is not beneficial to the performance of the hydrated layer, thereby reducing the surface mechanical properties of the matrix glass. Furthermore, as observed in Figure S7 in the Supporting Information, the optical transparency of the CsAlB glass significantly decreased upon aging at 23 °C with 60% RH due to the broken glass surface. However, surprisingly, there are no cracks inside this indent at the same applied load compared to the glass without aging (compare Figures 8c and 8d).

4. Discussion

The surface humid aging effect strongly depends on the inherent chemical durability of the glasses. The dissolution behavior is related to various factors such as atomic packing density, the rigidity of the network, modifier field strength, content of network formers (B_2O_3 and Al_2O_3), and, in particular, the network former speciation (fractions of B^{III} and B^{IV}). The dense network structure (high C_g) allows for less water penetration into the glasses, leading to lower D_r. Moreover, our previous work[26,34] has found the lower D_r values for glasses with high-field strength modifiers, which is in good agreement with the present results (Figure 2). In the LiAlB and KAlB glasses, relatively low D_r values (below 1 mg dm^{-2} h^{-1} in Figure 1) are observed in neutral (pH = 7) solutions due to their higher atomic packing density and modifier field strength compared to CsAlB glass (around 2.2 mg dm^{-2} h^{-1}). This explains why we observe a smaller degree of water penetration (below 1 wt%) in the LiAlB and KAlB glasses (powder) upon aging for 7 days. This suggests that the surface hydration should only have a minor effect on the mechanical properties of LiAlB and KAlB glasses under low-RH conditions. However, as reported in Table S2 in the Supporting Information, the LiAlB glass breaks upon treatment at 120 ℃ for 100% RH, while cracks starts to appear on the surface of the KAlB glasses after 1 day aging at 35 ℃ for 80% RH. In the case of the CsAlB glass, cracks occur on the surface already after 6 h aging at 23 ℃ for 60% RH. To better understand the effect of hydration on the crack initiation behavior, we also submerged the CsAlB glass in the 99.9% ethanol solution for two weeks. As shown in Figure S8 in the Supporting Information, impurity water from the ethanol apparently enters the glass to increase the OH content and slightly increase the *CR*. This again highlights the hygroscopic nature of the CsAlB glass.

The pristine CsAlB glasses consist of borate and aluminoborate structural units with large Cs cations encapsulated within the network, resulting in the relatively open structure (C_g=0.493). From the water content analysis, we find that this structure is prone to water penetration and attack, resulting in the breakdown of borate superstructures[20,21] and formation of Cs-OH groups with high mobility[21]. The water interaction with Cs modifiers suggests that water preferentially interacts with boron relative to aluminum (to form B^{IV}), while some of the Cs charge-compensators for Al^{IV} are removed by aging, effectively increasing the coordination number of aluminum[21]. Following Sheth *et*

al.,[51,52] we find that the formation of the hydration layer (network with high freedom and Cs-OH groups with high mobility as well as compressive stress[26]) on the surface of CsAlB glasses can have a large extent of densification and structural changes (mainly restructuring) during indentation, which can store or dissipate more energy from the applied load. Another possible effect could be that the micron-sized hydration layer will blunt the sharp contact area during the indentation process,[53] resulting in a smaller applied stress and thereby improving the crack resistance. In short, the existence of this hydration layer is important for achieving ultra-high crack resistance for the CsAlB glass, and thus better protect the glass from damage (Figure 8). To further investigate the effect of the hydration layer on obtaining ultra-high crack resistance, we studied the effect of post-aging heat treatment on *CR* of the hydrated CsAlB glasses (Figure S9 in the Supporting Information). *CR* of the aged glass is found to decrease approximately to its initial value (before aging) after heat treatment. This further confirms that the existence of the hydration layer is beneficial to improve the crack initiation resistance.

5. Conclusions

In this study, we have shown that the humid aging affects the indentation response of alkali aluminoborate glasses as a strong function of the alkali modifier field strength. The dense and rigid network structures of lithium and potassium glasses allow for less water penetration during the hydration process. Hence, the aqueous dissolution rate is below 1 mg dm^{-2} h^{-1} and the weight loss of powdered samples due to water uptake is below 1 wt% after humid aging for 7 days. As such, the surface hydration has only a minor effect on the indentation response (including bow-in parameter, side length recovery, hardness, and crack resistance) of the LiAlB and KAlB glasses. In contrast, humid aging has a significant effect on the mechanical properties of CsAlB glasses due to its higher aqueous dissolution rate (around 2.2 mg dm^{-2} h^{-1}) and higher water uptake in the powdered samples (above 10 wt%). Furthermore, Raman analysis has shown that the hydration layer depth after 7 days aging at 40% RH and 50% RH is 26.4 μm and 29.2 μm, respectively. The hydration layer has a network with higher freedom and Cs-OH groups with higher mobility. This gives rise to an ultrahigh

crack resistance (around 170 N) after aging for 7 days at 40% RH, but at the same time, this glass has a low hardness both before and after humid aging. Finally, we observed micron-sized shear bands inside the indent in the CsAlB glass upon aging at 60% RH.

Acknowledgements

This work was supported by the China Scholarship Council (CSC No. 201806370210).

References

1. Yao A, Wang D, Huang W, Fu Q, Rahaman MN, Day DE. In Vitro Bioactive Characteristics of Borate-Based Glasses with Controllable Degradation Behavior. J. Am. Ceram. Soc. 2007;90:303-306.
2. Donald IW, Metcalfe BL, Bradley DJ, Hill MJC, McGrath JL, Bye AD. The Preparation and Properties of Some Lithium Borate Based Glasses. J. Mater. Sci. 1994;29:6379-6396.
3. Veléz M, Tuller H, Uhlmann D. Chemical Durability of Lithium Borate Glasses. J. Non. Cryst. Solids 1982;49:351-362.
4. Zhang Z, Hirao K, Soga N. Water Corrosion Behavior of Densified Glass. II. Borate Glasses. J. Non. Cryst. Solids 1991;135:62-66.
5. Wiederhorn SM. Influence of Water Vapor on Crack Propagation in Soda-Lime Glass. J. Am. Ceram. Soc. 1967;50:407-414.
6. Takata M, Tomozawa M, Watson EB. Effect of Water Content on Mechanical Properties of Na_2O-SiO_2 Glasses. J. Am. Ceram. Soc. 1982;65:c156-c157.
7. Wiederhorn SM, Fett T, Rizzi G, Hoffmann MJ, Guin JP. The Effect of Water Penetration on Crack Growth in Silica Glass. Eng. Fract. Mech. 2013;100:3-16.
8. Fett T, Rizzi G, Hoffmann MJ, Wagner S, Wiederhorn SM. Effect of Water on the Inert Strength of Silica Glass: Role of Water Penetration. J. Am. Ceram. Soc. 2012;95:3847-3853.
9. Mei H, Yang Y, van Duin ACT, Sinnott SB, Mauro JC, Liu L, Fu Z. Effects of Water on the Mechanical Properties of Silica Glass Using Molecular Dynamics. Acta Mater. 2019;178:36-44.
10. Acocella J, Tomozawa M, Watson EB. The Nature of Dissolved Water in Sodium Silicate Glasses and Its Effect on Various Properties. J. Non. Cryst. Solids. 1984;65:355-372.
11. Tomozawa M, Takata M, Acocella J, Bruce Watson E, Takamori T. Thermal Properties of $Na_2O{\cdot}3SiO_2$ Glasses with High Water Content. J. Non. Cryst. Solids. 1983;56:343-348.
12. Deubener J, Müller R, Behrens H, Heide G. Water and the Glass Transition Temperature of Silicate Melts. J. Non. Cryst. Solids. 2003;330:268-273.
13. Griffith AA. The phenomena of rupture and flow in solids. Philos Trans R Soc London. 1921;221:163-98.

14. Seaman JH, Blanchet TA, Tomozawa M. Origin of the static fatigue limit in oxide glasses. J Am Ceram Soc. 2016;99:3600-9.

15. Charles RJ. Static fatigue of glass. I. J Appl Phys. 1958;29:1554-60.

16. Agarwal A, Tomozawa M, Lanford WA. Effect of Stress on Water Diffusion in Silica Glass at Various Temperatures. J. Non. Cryst. Solids. 1994;167:139-148.

17. Zhang Y, Stolper EM, Wasserburg GJ. Diffusion of Water in Rhyolitic Glasses. Geochim. Cosmochim. Acta. 1991;55:441-456.

18. Tomozawa M, Kim DL, Agarwal A, Davis KM. Water Diffusion and Surface Structural Relaxation of Silica Glasses. J. Non. Cryst. Solids. 2001;288:73-80.

19. Wiederhorn SM, Rizzi G, Wagner S, Schell G, Hoffmann MJ, Fett T. Diffusion of Water in Silica: Influence of Moderate Stresses. J. Am. Ceram. Soc. 2018;101:1180-1190.

20. Januchta K, Stepniewska M, Jensen LR, Zhang Y, Somers MAJ, Bauchy M, Yue Y, Smedskjaer MM. Breaking the Limit of Micro‐Ductility in Oxide Glasses. Adv. Sci. 2019;6:1901281.

21. Liu P, Youngman RE, Jensen LR, Bockowski M, Smedskjaer MM. Achieving Ultrahigh Crack Resistance in Glass through Humid Aging. Phys. Rev. Mater. 2020;4:063606.

22. Wiederhorn SM, Fett T, Rizzi G, Fünfschilling S, Hoffmann MJ, Guin JP. Effect of water penetration on the strength and toughness of silica glass. J Am Ceram Soc. 2011;94:s196-s203.

23. Gross TM, Sarafian AR, Wu J, Zheng Z. Water vapor strengthenable alkali-free glass compositions. U.S. Patent 015 699 5A1, 2020.

24. Gross TM, Guryanov GM. Water-Containing Glass-Based Articles With High Indentation Cracking Threshold. U.S. Patent 015 283 8A1, 2019.

25. Liu P, Januchta K, Jensen LR, Bauchy M, Smedskjaer MM. Competitive Effects of Free Volume, Rigidity, and Self‐adaptivity on Indentation Response of Silicoaluminoborate Glasses. J. Am. Ceram. Soc. 2020;103:944-954.

26. Januchta K, Bauchy M, Youngman RE, Rzoska SJ, Bockowski M, Smedskjaer MM. Modifier Field Strength Effects on Densification Behavior and Mechanical Properties of Alkali Aluminoborate Glasses. Phys. Rev. Mater. 2017;1:063603.

27. Wada M, Furukawa H, Fujita K. Crack resistance of glass on Vickers indentation. Proc Int Congr Glass. 1974;11:39-46

28. Yoshida S, Sanglebœuf JC, Rouxel T. Quantitative Evaluation of Indentation-Induced Densification in Glass. J. Mater. Res. 2005;20:3404-3412.

29. Januchta K, Liu P, Hansen SR, To T, Smedskjaer MM. Indentation Cracking and Deformation Mechanism of Sodium Aluminoborosilicate Glasses. J. Am. Ceram. Soc. 2020;103:1656-1665.

30. Mascaraque N, Frederiksen KF, Januchta K, Youngman RE, Bauchy M, Smedskjaer MM. Competitive Effects of Modifier Charge and Size on Mechanical and Chemical Resistance of Aluminoborate Glasses. J. Non. Cryst. Solids. 2018;499:264-271.

31. Dktzel A. Cation Field Intensities and Their Relation to Devimfication Phenomena, to Compound Formation, and to Melting Points of Silicates. Z. Elektrochem. Angew. Phys. Chemie. 1942;48:9-23.

32. Sun KH. Fundamental Condition of Glass Formation. J. Am. Ceram. Soc. 1947;30:277-281.

33. Makishima A, Mackenzie JD. Direct Calculation of Young's Moidulus of Glass. J. Non. Cryst. Solids. 1973;12:35-45.

34. Mascaraque N, Januchta K, Frederiksen KF, Youngman RE, Bauchy M, Smedskjaer MM. Structural Dependence of Chemical Durability in Modified Aluminoborate Glasses. J. Am. Ceram. Soc. 2019;102:1157-1168.

35. Wang B, Krishnan NMA, Yu Y, Wang M, Le Pape Y, Sant G, Bauchy M. Irradiation-Induced Topological Transition in SiO_2: Structural Signature of Networks' Rigidity. J. Non. Cryst. Solids. 2017;463:25-30.

36. Luo J, Huynh H, Pantano CG, Kim SH. Hydrothermal Reactions of Soda Lime Silica Glass-Revealing Subsurface Damage and Alteration of Mechanical Properties and Chemical Structure of Glass Surfaces. J. Non. Cryst. Solids. 2016;452:93-101.

37. Sheth N, Luo J, Banerjee J, Pantano CG, Kim SH. Characterization of surface structures of dealkalized soda lime silica glass using X-ray photoelectron, specular reflection infrared, attenuated total reflection infrared and sum frequency generation spectroscopies. J. Non. Cryst. Solids. 2017;474:24-31.

38. Luo J, Amma S, Chen L, Ngo D, Mauro JC, Pantano CG, Kim SH. Relative Abundance of Subsurface Hydroxyl and Molecular Water Species in Silicate and Aluminosilicate Glasses. J. Non. Cryst. Solids. 2019;510:179-185.

39. Peter KW. Densification and Flow Phenomena of Glass in Indentation Experiments. J. Non. Cryst. Solids. 1970;5:103-115.

40. Rouxel T, Ji H, Guin JP, Augereau F, Rufflé B. Indentation Deformation Mechanism in Glass: Densification versus Shear Flow. J. Appl. Phys. 2010;107:094903.

41. Yamane M, Mackenzie J. Vicker's Hardness of Glass. J. Non. Cryst. Solids. 1974;15:153-164.

42. Stepniewska M, Januchta K, Zhou C, Qiao A, Smedskjaer MM, Yue Y. Observation of Indentation-Induced Shear Bands in a Metal-organic Framework Glass. Proc. Natl. Acad. Sci. 2020;117:10149-10154.

43. Sellappan P, Rouxel T, Celarie F, Becker E, Houizot P, Conradt R. Composition Dependence of Indentation Deformation and Indentation Cracking in Glass. Acta Mater. 2013;61:5949-5965.

44. Hardiman M, Vaughan TJ, McCarthy CT. The Effects of Pile-up, Viscoelasticity and Hydrostatic Stress on Polymer Matrix Nanoindentation. Polym. Test. 2016;52:157-166.

45. Yoshida S, Kato M, Yokota A, Sasaki S, Yamada A, Matsuoka J, Soga N, Kurkjian CR. Direct Observation of Indentation Deformation and Cracking of Silicate Glasses. J. Mater. Res. 2015;30:2291-2299.

46. Smedskjaer MM, Mauro JC, Yue Y. Prediction of Glass Hardness Using Temperature-Dependent Constraint Theory. Phys. Rev. Lett. 2010;105:115503.

47. Greer AL, Cheng YQ, Ma E. Shear Bands in Metallic Glasses. Mater. Sci. Eng. R Reports. 2013;74:71-132.

48. Lu YM, Sun BA, Zhao LZ, Wang WH, Pan MX, Liu CT, Yang Y. Shear-Banding Induced Indentation Size Effect in Metallic Glasses. Sci. Rep. 2016;6:28523.

49. Gross TM, Wu J, Baker DE, Price JJ, Yongsunthon R. Crack-Resistant Glass with High Shear Band Density. J. Non. Cryst. Solids. 2018;494:13-20.

50. Ernsberger FM. Mechanical Properties of Glass. J. Non. Cryst. Solids. 1977;25:293-321.

51. Sheth N, Hahn SH, Ngo D, Howzen A, Bermejo R, van Duin ACT, Mauro JC, Pantano CG, Kim SH. Influence of acid leaching surface treatment on indentation cracking of soda lime silicate glass. J. Non. Cryst. Solids. 2020;543:120144.

52. Sheth N, Greenley C, Bermejo R, Mauro JC, Pantano CG, Kim SH. Effects of acid leaching treatment of soda-lime silicate glass on crack initiation and fracture. J. Am. Ceram. Soc. 2021;00:1-9. https://doi.org/10.1111/jace.17840

53. Rouxel T, Yoshida S. The fracture toughness of inorganic glasses. J. Am. Ceram. Soc. 2017;100:4374-4396.

FIGURE CAPTIONS

Figure 1. (a) Alkali field strength (*FS*) and (b) atomic packing density (C_g) dependence on the logarithmic dissolution rate (D_r, in mg dm^{-2} h^{-1}) in the neutral (pH = 7) solution.

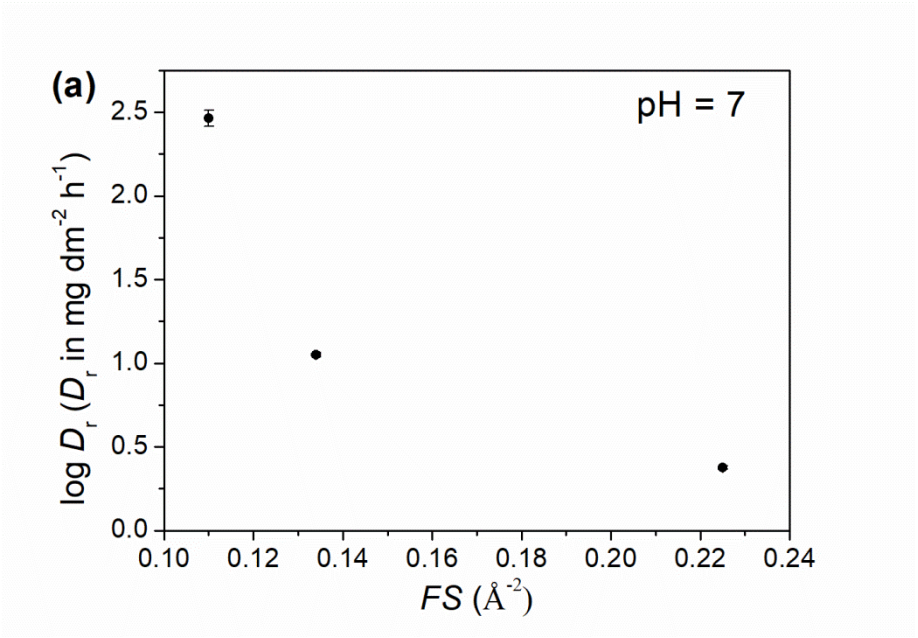

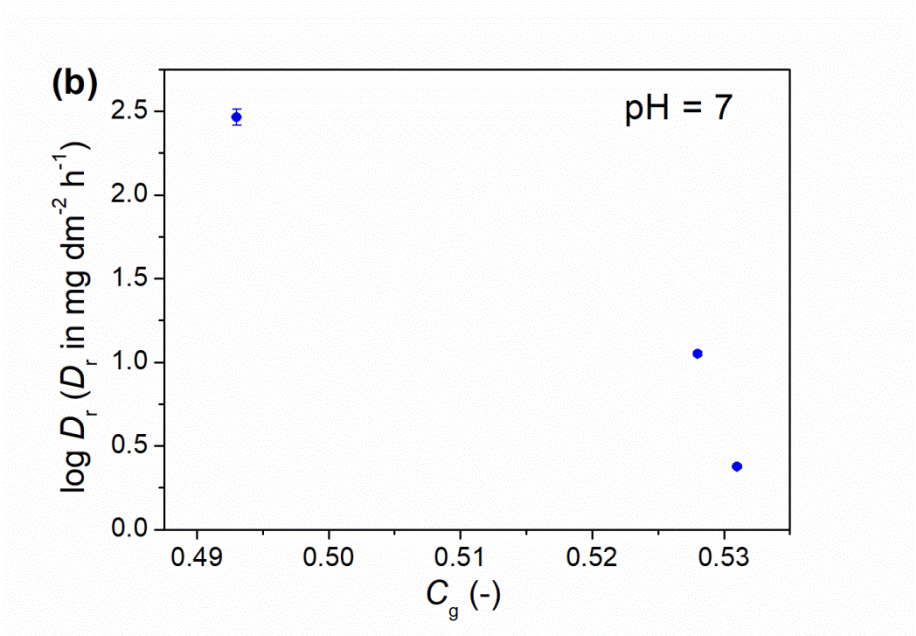

Figure 2. (a) ATR-IR spectra of LiAlB glass with different aging time at 23 °C, 80% RH. (b) ATR-IR spectra of KAlB glass with different aging time at 23 °C, 80% RH. (c) ATR-IR spectra of CsAlB glass with different aging time at 23 °C, 50% RH. (d) Relatively intensity of OH stretching band (around 3400 cm^{-1}) as a function of humid aging time of the studied glasses at different RHs.

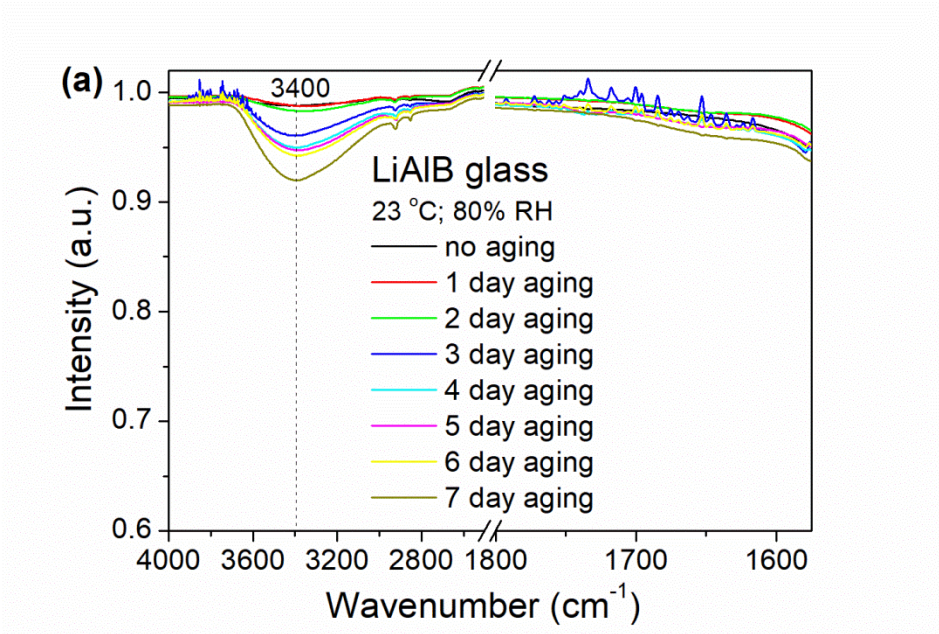

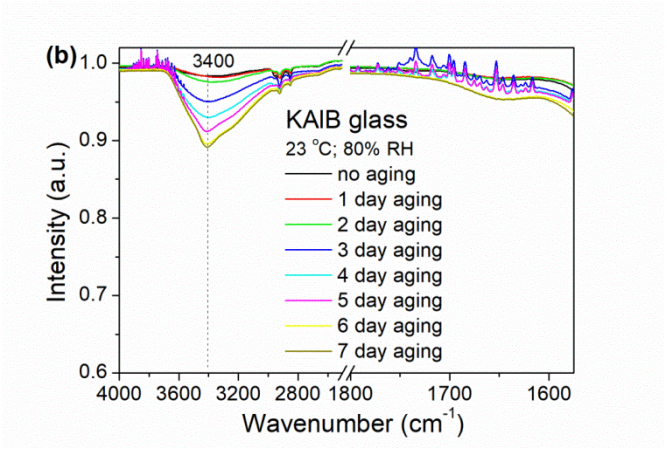

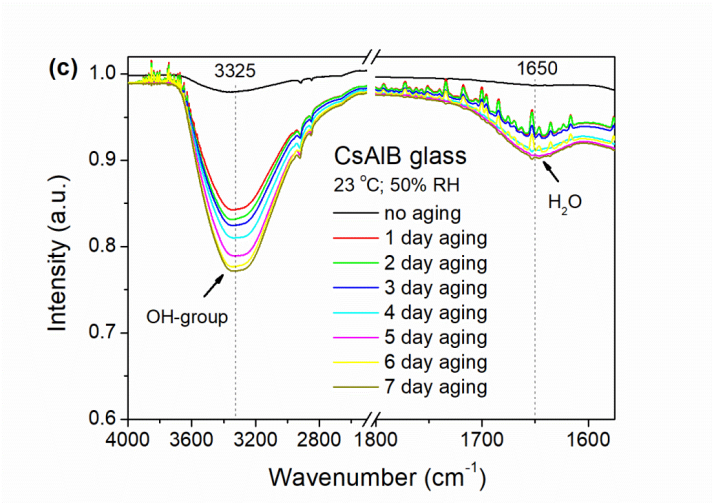

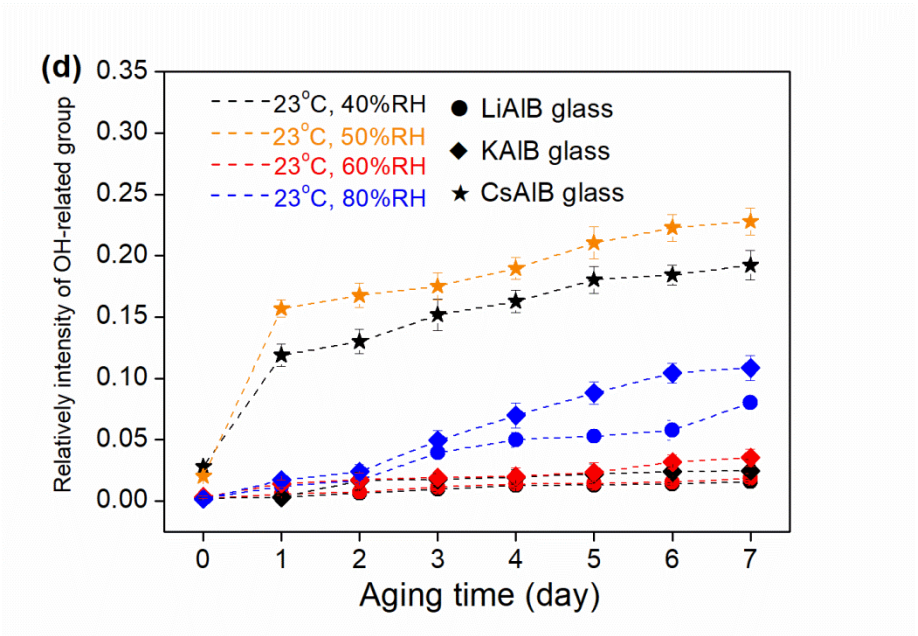

Figure 3. (a) Micro-Raman spectra of CsAlB glass after aging for 7 days at 50% RH. The spectra were recorded at increasing depth from the top surface toward the inside of the glass. (b) The area ratio of band Ⅰ and Ⅱ (from figure a) as a function of depth for CsAlB glass. The experimental data is fit to an exponential function (solid line) and the hydration layer is defined as the depth for which the slope of the curve is less than -0.01 μm^{-1}. (c) Hydration layer depth as obtained from micro-Raman spectra as a function of humid aging time for the CsAlB glasses under 40% and 50% RH.

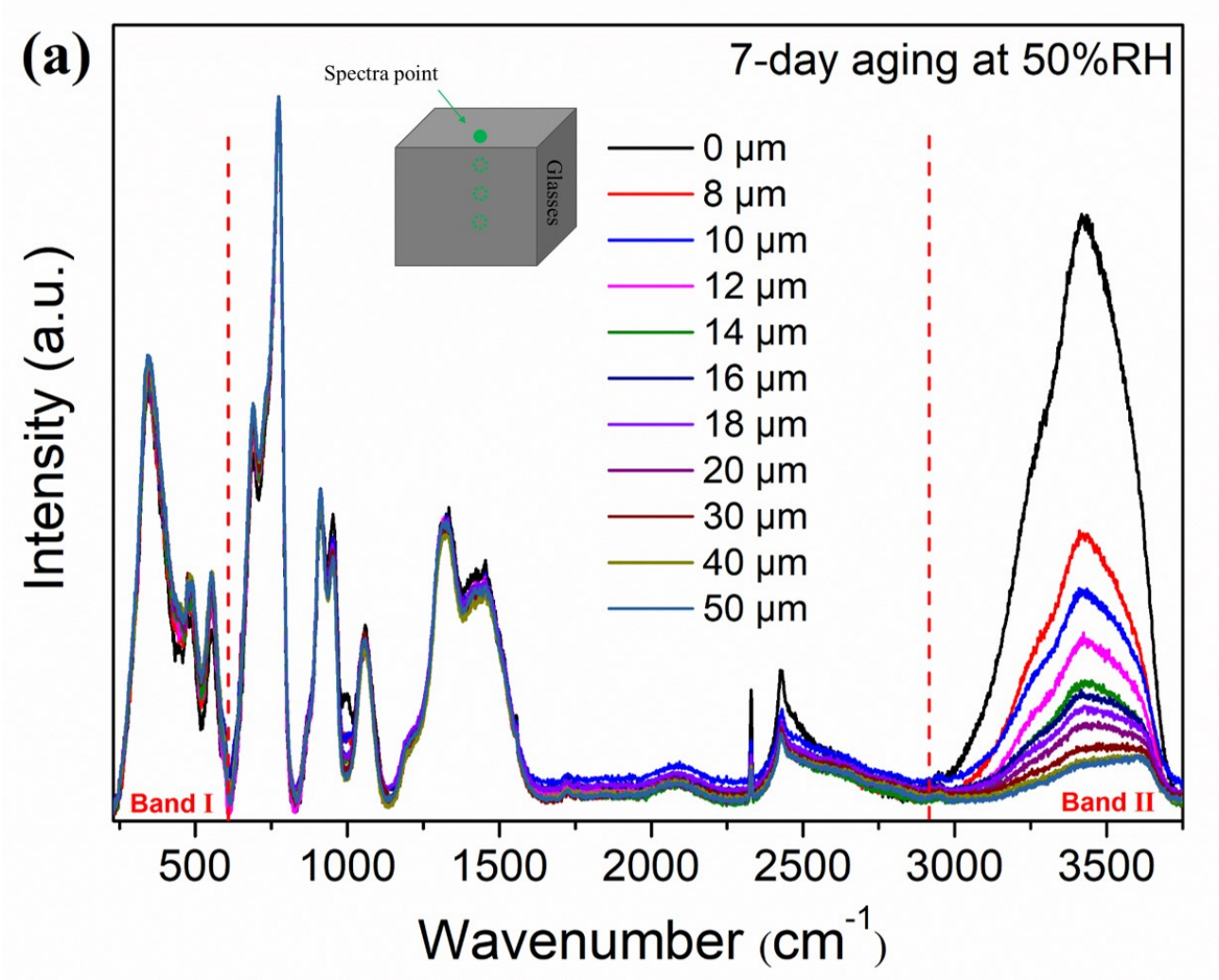

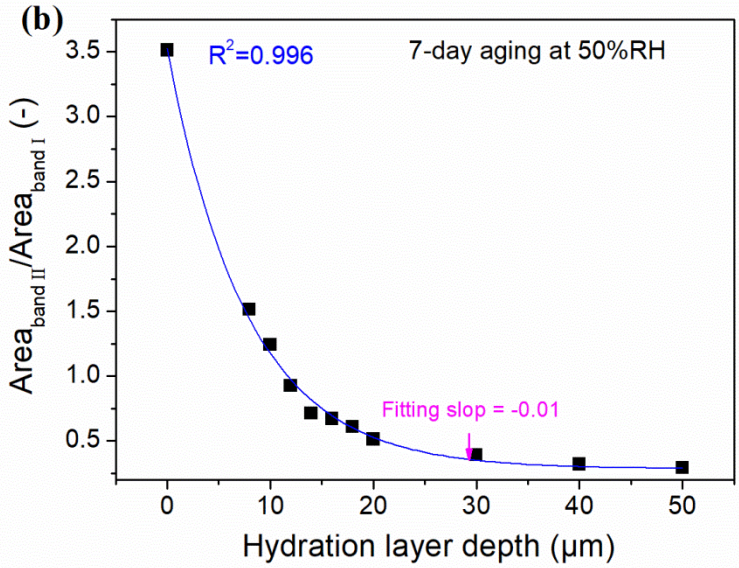

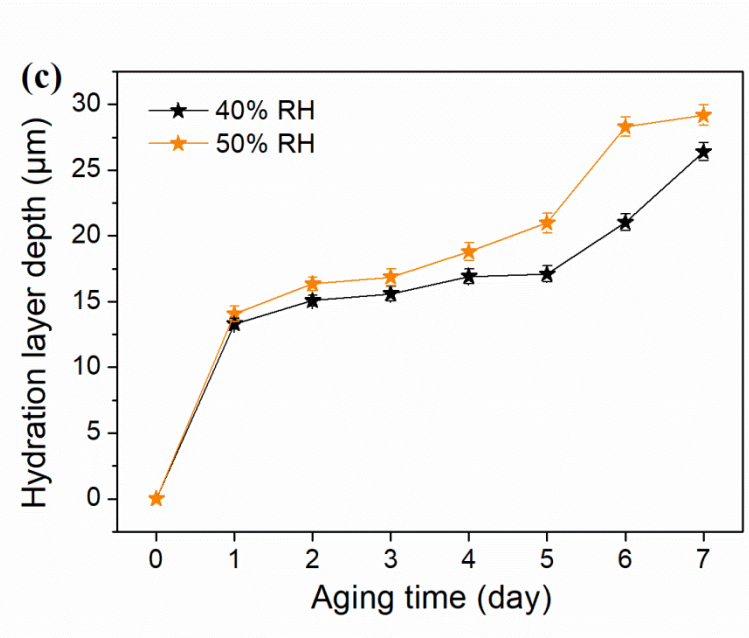

Figure 4. Dependence of the bow-in parameter (L_D/L_S ratio) of Vickers indents produced at 9.8 N on the humid aging time for different glasses and RHs.

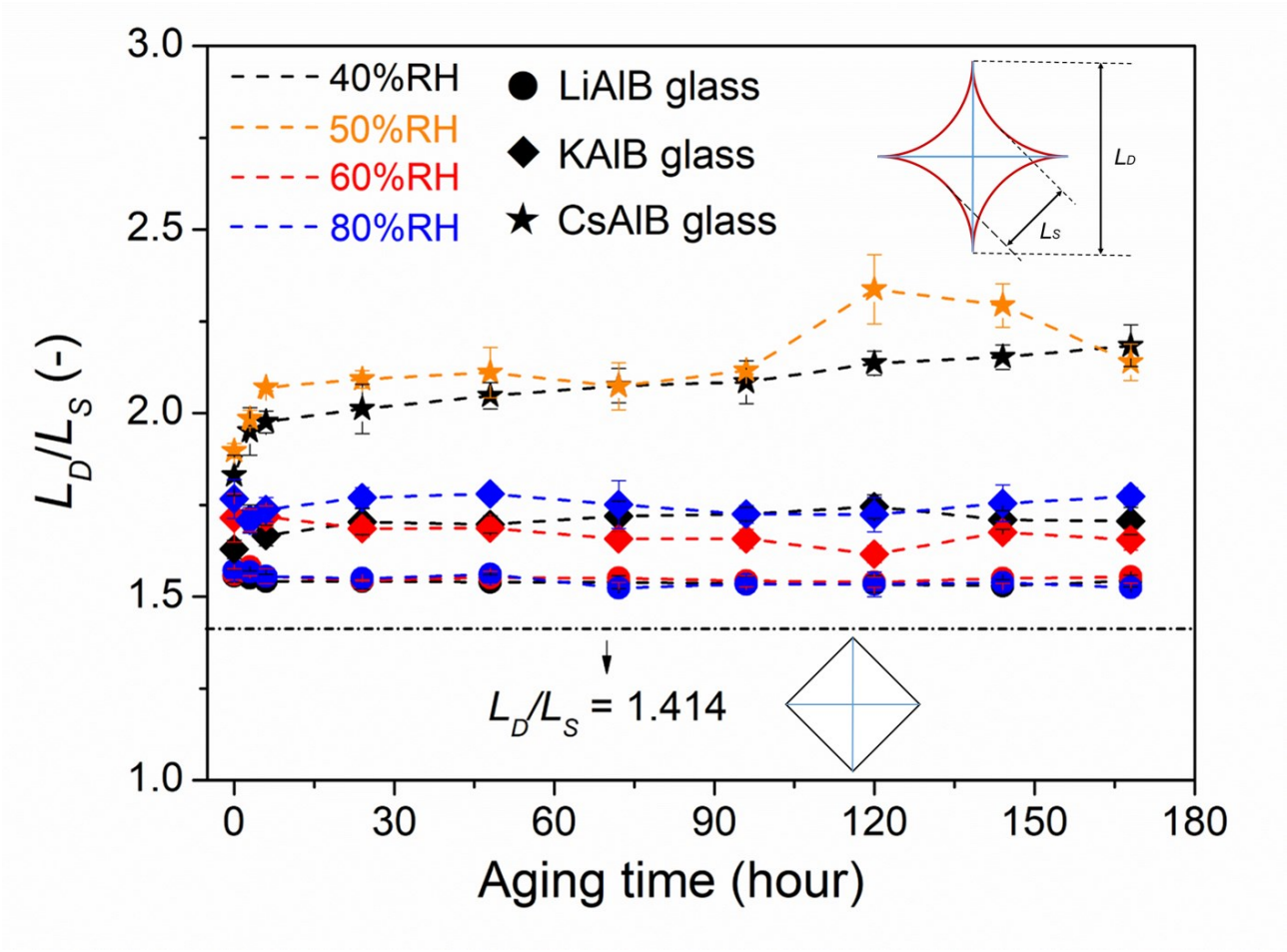

Figure 5. Side length recovery (L_{AR}) of Vickers indents produced at 9.8 N as a function of humid aging time for the investigated glasses under various RHs.

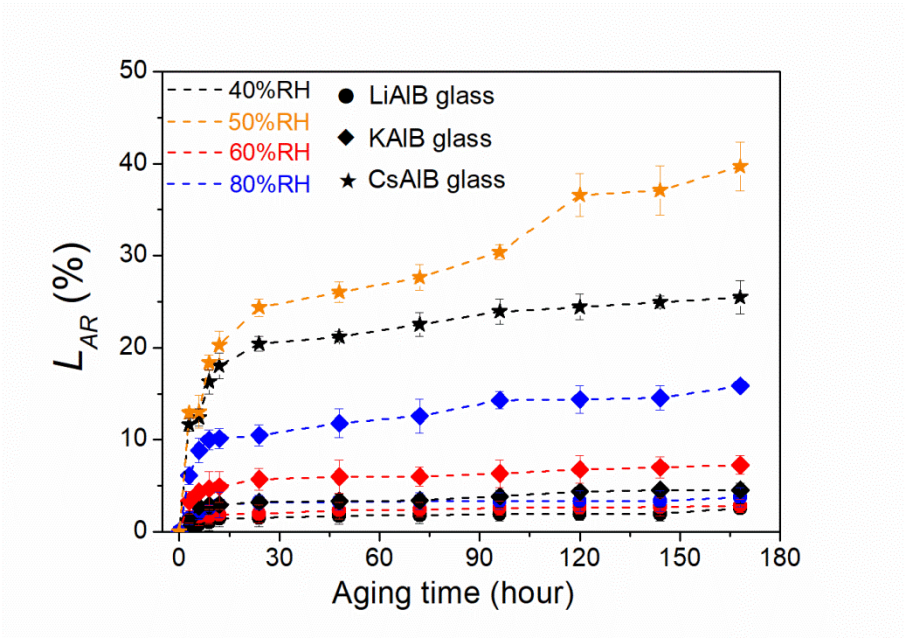

Figure 6. Dependence of the Vickers hardness of indents produced at 9.8 N on the humid aging time for different glasses and RHs.

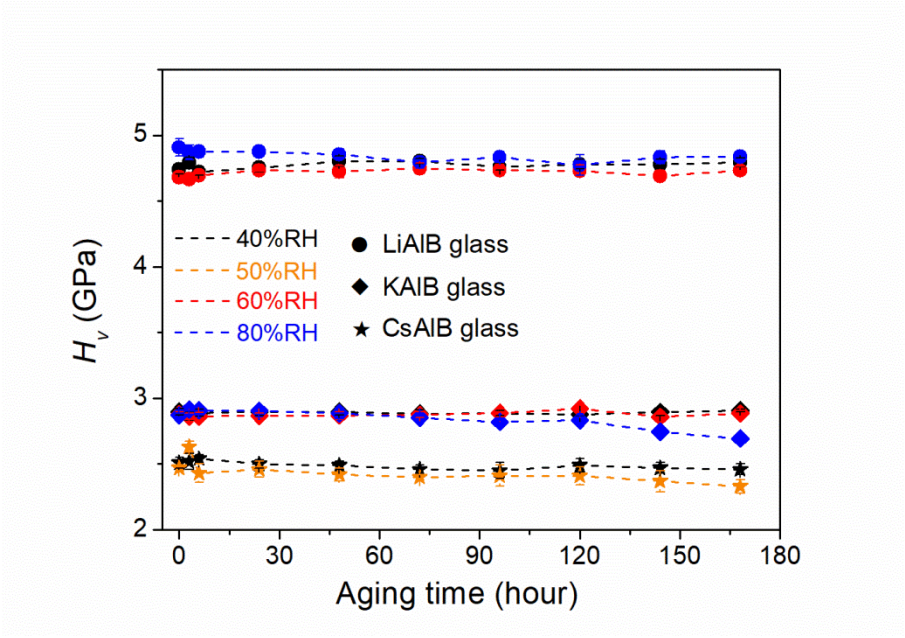

Figure 7. Dependence of crack resistance (*CR*) on the humid aging time for different glasses and relative humidities. The estimated error in crack resistance is around ± 20%.

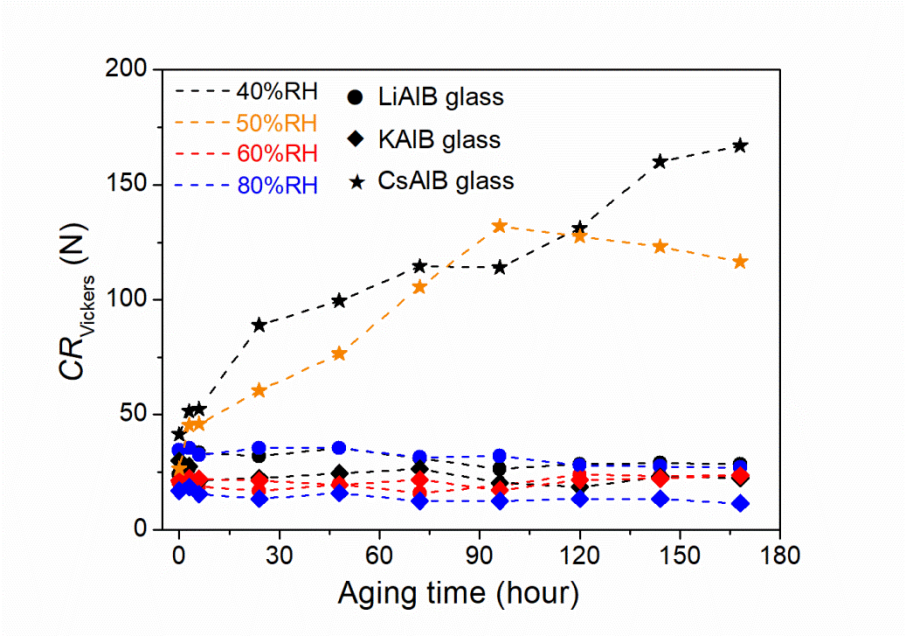

Figure 8. Optical images of Vickers indents produced at different loads on the surface of the CsAlB glass before and after humid aging at 60% RH. (a) Indentation at 9.8 N without aging. (b) Indentation at 9.8 N after 3 hours aging. (c) Indentation at 40 N without aging. (d) Indentation at 40 N after 3 hours aging.